Energy Conversion and Management: X 27 (2025) 101156

Contents lists available at ScienceDirect

Energy Conversion and Management: X

journal homepage: www.sciencedirect.com/journal/energy-conversion-and-management-x

From organic rankine cycles to high-temperature heat pumps: A thermo-economic investigation of potential working fluids

Echezona Obika [a,b,*], Florian Heberle [a], Dieter Brüggemann [a]

[a] Chair of Engineering Thermodynamics and Transport Processes (LTTT), Center of Energy Technology (ZET), University of Bayreuth, Universitätsstraße 30, 95447 Bayreuth, Germany
[b] Department of Mechanical Engineering, Nnamdi Azikiwe University, Awka, P.M.B. 5025, Awka, Anambra State, Nigeria

ARTICLE INFO

Keywords:
Cyclohexane
COP
Vapor compression
Waste heat
Supply temperature
Levelized cost of heat

ABSTRACT

The thermo-economic performance of high-temperature heat pump utilizing working fluids applied to ORC systems with high critical temperatures like cyclohexane, hexane and cyclopentane were compared to intensively examined working fluids, in this study. The aim is to determine their economic feasibility for high temperature supply up to 150 °C. The vapor compression cycle with internal heat exchanger was adopted for this evaluation, for a heat source of 50 °C, supply temperatures in the range of 100 to 150 °C and heat exchanger pinch point temperature difference of 5 K. The coefficient of performance (COP) of the cycle was optimized at the considered boundary condition by attaining maximum subcooling at the condenser. A 7.9 % higher COP was obtained with cyclopentane compared to the state-of-the-art working fluid R1336mzz(Z). From the economic point of view these cyclic hydrocarbons, especially cyclopentane, are associated with 1.5 % higher specific investment cost. However, these working fluids lead to 5 % discounted payback period due to increased performance, compared to R1336mzz(Z). These positive results affirm the prospect of cyclopentane as a suitable working fluid for heat pump applications both from the thermodynamic and economic point of view.

1. Introduction

The demand for heat provision is relevant across all sector of the economy, spanning from process heat in manufacturing [1–3], to heat requirements for district heating [4,5]. Studies have indicated that heat pumps have significant potential for providing heat at different temperatures in these sectors, with a technical potential of 113 PJ of process heat up to 150 °C in the European market alone [6]. They are suitable for recovering waste heat, capable of delivering district heat in the range of 30 to 40 °C waste steel process heat at I0 MW installed capacity in Angang Lingshan steel plant of China, as per the study of Hu et al. [7]. This also includes the effective utilization of waste at different temperature to provide energy required for dyeing process [8]. Furthermore, research by Zhao et al. [9] on waste heat recovery using heat pump demonstrated the potential to produce steam at 85 °C evaporating temperatures. The potential for completely environmentally friendly operation through heat pumps makes it a preferred option in today's society compared to the use of fossil fuels in gas burners [10]. An extensive review by Jiang et al. [11,12] supports the development of high-temperature heat pumps (HTHP) with source temperature of 30 °C and supply temperatures up to 100 °C. The claim of a possible replacement for gas burners is further strengthened by the proposed 140 °C steam generation at a COP of 2.7, as concluded from the HTHP analysis by Ma et al. [13]. Zühlsdorf et al. [14], identified the potential to supply process heat up to 280 °C using electrically driven heat pumps. Environmental concerns related to heat pump use are being addressed through ongoing research on the selection of working fluids [15]. Li et al. [16] recommended R365mfc and R1233zd(E) as the best replacement for R245fa, which has been phased out due to high ozone depletion potential. Previous research [17] has shown that natural working fluids such as cyclohexane, have high performance capabilities. The study of Di et al. [18] has confirmed that HTHP technologies with R718 as refrigerant not only meet high temperature requirements but also deliver the best system performance. This has led to the adaptation of more environmentally friendly working fluids to replace those with harmful effects like chlorofluorocarbons (CFCs) and hydrochlorofluorocarbons (HCFCs) [6,11,19]. A study of 16 working fluids on 10 HTHP configurations by Andersen et al. [20], highlighted the potential of sustainable high-temperature heat pump application with natural working fluids. Natural working fluids are most preferred for achieving minimal environmental impact and are the focus of recent

* Corresponding author.
E-mail address: Echezona.Obika@uni-bayreuth.de (E. Obika).

https://doi.org/10.1016/j.ecmx.2025.101156
Received 9 June 2025; Received in revised form 16 July 2025; Accepted 17 July 2025
Available online 18 July 2025

Nomenclature

$\dot{A}$	area (m^2)
B_1B_2	are empirical factors
B_o	boiling number
K_1, K_2K_3	equipment cost factors
$\dot{Q}$	heat transfer (kW)
$\dot{m}$	mass flowrate (kgs^{-1})
h	enthalpy ($kjkg^{-1}$) or heat transfer coefficient ($kwm^{-2}k^{-1}$)
CE	component cost (€)two-phase convection multiplier
H	heat (kw)
K	thermal conductivity of fluid ($kwm^{-1}k^{-1}$)
N	yearly operating hours (hours)
P	pressure (bar)
Pr	prandtl number
Re	reynolds' number
S	entropy
T	temperature (^{o}c)
U	overall heat transfer coefficient ($kwm^{-2}k^{-1}$)
W	work (kw)
$dorD$	diameter (m)
i	interest rate (%)
x	vapor fraction
λ	thermal conductivity of tube ($kwm^{-1}k^{-1}$)

Greek letters

η	efficiency
Δ	difference
$<$	less than
Σ	summation

Superscripts

o	base case

Abbreviations

COP	coefficient of performance
DPBP	discounted pay back period
HC	hydrocarbon
HFO	hydrofluoroolefin
HTA	heat transfer area
HTHP	high temperature heat pump
IHX	internal heat exchanger
LCOH	levelized cost of heat
NPV	net present value
SEC	speccifi equipment cost
SIC	specific investment cost
TCI	total cost of investment
TEC	total equipment cost

Subscripts

2p	two-phase
c	cold
Comp	compressor
Cond	condenser
crit	critical
des	desuperheat
dis	discharge
eva	evaporator
f	liquid
h	hot
hx	heat exchanger
is	isentropic
NB	nucleate boiling
r	ratio
sh	shell
sp	single phase
sub	subcool
sup	supply
tub	tube

research studies [11,21–23]. In addition to environmental considerations, the costs associated with integrating heat pumps must be assessed to determine their feasibility [24]. Hence, an effective selection of working fluid for a specific application will be based on a balanced compromise between efficiency and associated costs. Moreover, with the idea of heat pumps as a replacement for gas burners [6,13], it is important to determine the cost savings resulting from such replacement [21].

Thermo-economic analysis has been carried out on heat pumps using different working fluids in various research studies. Jeßberger et al. [25] examined the effects of upscaling laboratory heat pumps using R1233zd (E) and found a 15 % increase in losses, along with up to 3.5 % and 8.7 % increase in volumetric and isentropic efficiencies, respectively, with a 3.2 scale-up factor. For temperatures up to 200 °C, Spale et al. [26] suggested a blend of cyclopentane and R1336mzz(Z) as the most optimal option in terms of performance and safety balance. Kosmadakis et al. [19] researched the feasibility of synthetic working fluids to upgrade waste heat up to 150 °C and concluded that the HFO R1234ze(Z) seems to be more promising with a high cycle performance and heating capacity compared to R1233zd(E) and R1336mzz(Z). However, due to its low production limit of 140 °C for HFO R1234ze(Z) in a single stage cycle, R1335mzz(Z) has been suggested for high temperature ranges. Vannoni et al. [27] indicated that *iso*-butane has potential for HTHP for waste heat recovery, especially for temperatures not exceeding 120 °C, from a techno-economic standpoint, with the compressor being the major contributor to the total investment cost. Vieren et al. [28] analyzed the integration of pure and binary working fluids for high-temperature heat pumps from the economic point of view, considering source temperatures of up to 120 °C over supply temperatures up to 200 °C. The results proved that pure fluids are more promising for operations with large temperature glides between the source and the sink. Hosseinnia et al. [29] justified the viability of R600 and R718 in a cascaded heat pump system, delivering heat up to 150 °C. The review of Arpagaus et al. [6] on the application potentials of refrigerants reported a specific cost of 200 to 800 €/kW for HTHP depending on factors such as plant size, refrigerant, heat sink, and source. A summary of relevant studies is presented in Table 1.

One consistent finding in existing techno-economic studies is that the specific equipment cost of heat pump systems depend strongly on several factors, including working fluids and boundary conditions [6]. However, most published studies focus on working fluids with critical temperatures below 200 °C and target heat supply temperatures under 130 °C. This narrow focus limits the development of high-temperature heat pumps (HTHPs) that can supply heat at higher temperatures using environmentally friendly fluids. While cyclic hydrocarbons have demonstrated promising thermal performance in Organic Rankine Cycle (ORC) systems [30,31] — for example, Abbas and Vrabec [32] reported thermal efficiencies of 19.13 % and 18.03 % for cyclohexane and cyclopentane respectively— their potential as working fluids for HTHPs remains largely unexplored. This represents a clear knowledge gap, as no comprehensive thermo-economic assessment exists for integrating cyclic hydrocarbons with high critical temperatures into HTHPs.

Therefore, the primary goal of this study is to fill this gap by investigating the performance and economic feasibility of using cyclic

Table 1
Summary of relevant studies.

Reference	Working fluid	method	Source temp (°C)	Supply temp (°C)
Doninelli et al. [33]	Fluorobenzene	Theoretical	70—130	180
Wei et al. [34]	R1234ze(E)	Experimental	−5–10	50
Wei et al. [35]	R32	Theoretical	18	50–60
Bergamini et al. [36]	R290, R600a, R717, R718	Theoretical	20–80	180
Andersen et al. [20]	R170, R290, R600, R600a, R601, R601a, R602, RE170, R717, R718, R744, R1224yd(Z), R1233zd(E), R1234ze(E), R1234ze(Z), R1336mzz(Z)	Theoretical	0–100	250
Obika et al. [17]	Cyclohexane, MM, cyclopentane, cyclopropane, R600, R600a, R601, R601a, R1336mzz(Z), R1234ze(Z), R1233rd(E)	Theoretical	50	140–170
Navarro-Esbri and Mota-Babiloni [37]	R1336mzz(Z)	Experimental	83–117	102–158
Ma et al. [38]	MC-1, HFC245fa, HFC245ca, HFC236ea, HFC1234ze(Z), HFC142b	Theoretical	60	85–120
Ommen et al. [39]	R290, R744, R717, R600a, R134a	Theoretical	–	120
Suong and Asanakham [40]	R152a, R124, R125, R134a, R143a, R1234yf, R1234ze (E), R290, R218, R32, R600, R717, R1270	Theoretical	−10–5	35–65
Vieren et al. [41]	Cyclobutene, Cis-2-butene	Theoretical	–	200
Mateu-Royo [42]	R245fa	Experimental	60–80	90–140
Lu et al[43]	R141b	Theoretical	45–70	105–130
Kosmadakis et al. [19]	R1233zd(E), R1336mzz(Z), R1234ze(Z)	Theoretical	<100	150
Vannoni et al. [27]	R600a	Theoretical	70	120
Wu et al. [44]	R410a, R245fa	Experimental Theoretical	−20–43	125

hydrocarbons in high-temperature heat pump cycles. Specifically, this research compares these hydrocarbons with well-established fluids such as R601, R601a, and R1336mzz(Z) in classically optimized HTHP configurations. The study focuses on heat supply temperatures up to 150 °C, aiming to identify environmentally benign working fluids that can expand the viable operating range of HTHPs.

In doing so, this work addresses the following research questions:

- How do the performance characteristics of cyclic hydrocarbons compare with conventional working fluids in an optimized HTHP cycle?
- How economically competitive are these cyclic hydrocarbons relative to commonly used alkanes and HFOs?

2. Method

2.1. HTHP cycle

The Aspen Plus software was used to model the vapor compression heat pump with internal heat exchanger configuration [45,46], depicted in Fig. 1. This setup comprises the evaporator, compressor, condenser, internal heat exchanger (IHX), and expansion valve. The working fluid is evaporated to a vapor fraction of 1 at state point 1, then gets superheated to point 2 by the IHX at the entrance of the compressor. On exiting the compressor at point 3, it undergoes compression to high pressure and temperature. Within the condenser, the working fluid experiences desuperheating, condensation, and subcooling processes, exiting at point 6 as subcooled liquid, while transferring heat to the sink. The fluid is additionally subcooled in the IHX to point 7 and then expanded to low pressure at point 8. The low-pressure double-phase fluid returns to the evaporator to continue the cycle.

2.2. Selection of operating parameters

This section presents the criteria for the selection of the boundary conditions and the working fluids adopted in the study.

2.2.1. Selection of boundary conditions

The heat source is simulated as water with a constant temperature and pressure of 50 °C and 5 bar respectively. This temperature is typical for industrial waste heat recovery [47], which is an efficient heat source for heat pumps [48–50]. The heat sink is modelled as water with a constant inlet pressure of 15 bar, to ensure the sink outlet remains in the liquid state. The sink outlet temperature is modelled as pressurized water up to 150 °C, encompassing various process heat temperature requirements, particularly in the chemical, paper, and metal industries [51,52]. The evaporator is modelled to completely vaporize the working fluid, while the superheat requirement for the fluids is addressed in the IHX to increased efficiency [53]. The condenser is considered as a compact heat exchanger to handle the desuperheating, condensing and subcooling requirements of the cycle. A minimum pinch point temperature difference of 5 K is predetermined for all heat exchangers. Both heat and pressure loss were not considered in the simulation. The boundary conditions are detailed in Table 2, mostly adopted from previous investigation [17].

2.2.2. Selection of working fluids

This economic analysis considered five different working fluids—four natural refrigerants and one synthetic fluid — as outlined in Table 3. The fluid selection process primarily relied on a good performance index, as indicated in a previous publication [17]. Working fluids with critical temperatures below 170 °C were excluded to enable subcritical operation for supply temperatures up to 150 °C. In addition, the selection accounted for the slope of the saturation vapor line on the *T,s*-diagram (see Fig. 2), focusing on dry and isentropic fluids, which are well-suited for stable cycle operation.

From an environmental perspective, the selected fluids exhibit low global warming potential (GWP < 10) and zero ozone layer depletion potential (ODP). Another important factor is their classification regarding per- and polyfluoroalkyl substances (PFAS). Increasing scientific and regulatory attention is being paid to PFAS due to their persistence and potential to form harmful degradation products such as trifluoroacetic acid (TFA), which can contaminate water sources [54]. Consequently, proposed legislation in the European Union and other regions aims to restrict or ban the use of fluorinated substances that fall under the broad PFAS definition. If implemented, such bans could significantly affect the availability and acceptability of certain hydrofluoroolefins (HFOs), and hydrofluorocarbons (HFCs) commonly used in heat pump, air-conditioning and refrigeration as well as ORC systems.

In this context, the use of natural hydrocarbons, such as

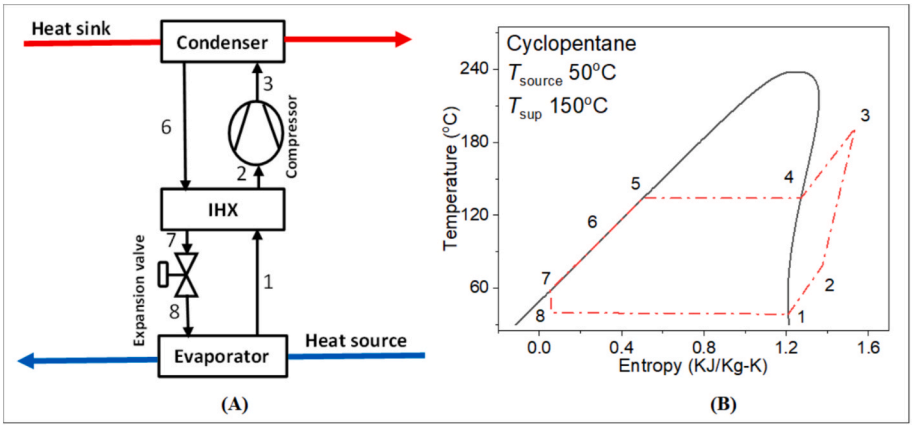

Fig. 1. Schematic scheme of the considered vapor compression heat pump cycle with IHX and corresponding *T,s*-diagramm.

Table 2
Boundary conditions.

Parameters	Constant value	Range
Heat source inlet temperature	50 °C	
Heat source temperature glide	5 °C	
Heat sink temperature glide		50–100 °C
Heat sink outlet temperature		100–150 °C
Heat source pressure	5 bar	
Heat sink pressure	15 bar	
ΔT_{PP} (all heat exchangers)	5 K	

cyclopentane and cyclohexane, gains additional relevance because they do not contain fluorine and are not subject to PFAS-related restrictions. Although R1336mzz(Z) is a fluorinated fluid that technically falls under the PFAS classification [54], it has been shown to have a very low risk of forming TFA [55] and is considered a relatively safe alternative to high-GWP HFCs like R245fa [56,57]. Nevertheless, future regulatory developments may tighten restrictions on all PFAS-classified refrigerants, further underscoring the importance of exploring non-fluorinated working fluids for high-temperature heat pump and ORC applications.

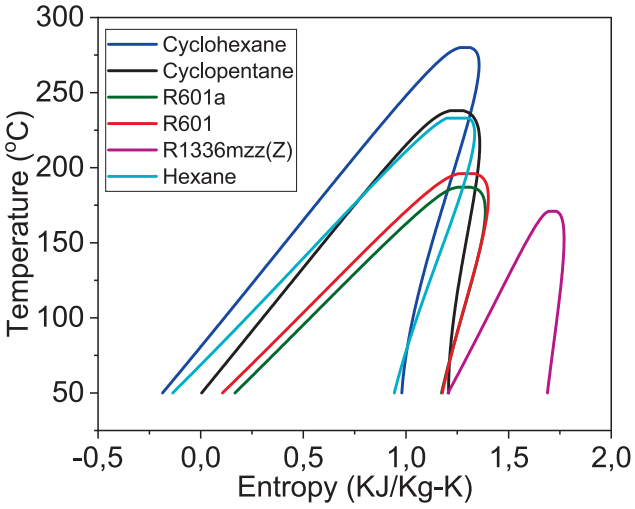

Fig. 2. T, s diagram of the selected working fluids from REFPROP [58].

2.3. Thermodynamic modelling

The thermodynamic modelling of the system was done using Aspen plus V12.1. Different solvers (model blocks) in the Aspen Plus V12.1 software, were selected to compute the mass and energy balance of the various components as presented in Table 4. The HeatX block was selected for all the heat exchangers. This solver enables the division of the heat exchanger into 100 zones to facilitate an accurate setting of the pinch point temperature difference ΔT_{pp}. The isentropic compressor block selected for the compressor performs vapor–liquid checks through the compression process. This enables the identification of wet

Table 4
Selected solvers.

Components	Solver	Governing equation	Reason
Evaporator, IHX and condenser	HeatX	$\dot{Q} = \dot{m}C_p\Delta T$	Performs zone analysis, Sets ΔT_{pp}, calculates quantity of heat transfer
Compressor	Isentropic compressor	$\eta_{is}\Delta h = \Delta h_s$	Calculates input power, performs vapor–liquid check
Expansion valve	Valve block	$\Delta h = 0$	Adiabatic flash

Table 3
Working fluid properties.

Fluids	Type	**ODP	**GWP (100 yr)	*T_crit (°C)	*p_crit (bar)	***Safety Class	Slope type
Cyclohexane	HC	0	~20	280.7	40.8	A3	Dry
Cyclopentane	HC	0	<25	238.6	45.1	A3	isentropic
Hexane	HC	0	<1	234.29	30.25	A3	Dry
n-Pentane (R601)	HC	0	<1	196.6	33.6	A3	Dry
Isopentane (R601a)	HC	0	<1	187.8	33.8	A3	Dry
R1336mzz(Z)	HFO	0	2	171.3	29.0	A1	isentropic

*The thermodynamic properties were obtained from REFPROP 10.0a database[59].
**ODP and GWP are according to WMO 2022 scientific report on ozone depletion [60], U.S. Environment Protection Agency (EPA) [61], Abbas and Vrabec [32] and Zhai et al. [62].
***safety class is evaluated to ANSI/ASHARAE[63].

compression at any point in the compression process. The valve block selected for the expansion valve, calculates adiabatic flash for the determined outlet pressure. The given set of equations applies to the system under steady-state conditions. The flow chat summarizing the study is presented in Fig. 3.

2.3.1. Compressor

The isentropic compressor model was utilized to represent the compressor. This model block offers the flexibility to specify either the discharge pressure, pressure ratio, pressure increase, or required power, with a single degree of freedom. In this instance, the discharge pressure was adjusted through the software's design specification function to achieve the desired 5 K pinch point temperature difference at the condenser. Equation (1) presents the compressor energy balance equation. The isentropic efficiency was estimated by fitting the inlet volume flowrates and volume ratios, in the screw expression suggested by Astolfi [64].

$$\eta_{is} = a\left[b + c\ln\dot{v}_{in} - dv_r\right] \tag{1}$$

$$a = 1 - 0.264\ln(v_r/7) \tag{2}$$

The fitted constants (b, c, and d) are 0.9403305, 0.0293295 and 0.0266298 respectively. $\dot{v}_{in}$ is the suction volume flow rate and v_r is the volume ratio.

The model was validated using empirical data from a screw compressor, thereby confirming its applicability to the present study. This was fitted into the compressor model using the calculator block provided by the software. Unlike several other isentropic efficiency expressions considering just the pressure ratios, the volume ratio and inlet volumetric flow rate captures the quantity of the fluid that passes through the compressor. This compressor model is compatible with different working fluids because it explicitly accounts for the fluid's thermodynamic and volumetric behaviour through the inlet volumetric flow rate and the internal volume ratio. Both parameters are strongly dependent on the working fluid's properties — including density, compressibility, and saturation conditions. By using this fitted correlation, the isentropic efficiency adapts automatically when a new fluid changes the suction flow rate and required volume ratio. This ensures that the compressor's performance prediction reflects the real impact of switching to a fluid with different vapor density or molecular weight. Importantly, the original work by Astolfi [64], validated this correlation for more than thirty different working fluids — including hydrocarbons and other organic fluids commonly used in heat pumps and ORC applications. This broad validation range demonstrates that the model reliably captures how changes in fluid properties affect compressor behaviour across a wide spectrum of refrigerant types.

Therefore, the present study can robustly assess the effect of switching to different working fluids within the same compressor design concept. In practice, the simulation adjusts the discharge pressure and resulting flow conditions to meet the cycle target. This ensures realistic energy balances and performance predictions when comparing multiple fluids at the screening stage.

In addition to the isentropic efficiency, the compressor's volumetric efficiency was explicitly modelled to account for internal leakage and re-expansion losses, which significantly influence the actual suction flow rate. The volumetric efficiency was estimated using the empirical correlation proposed by Fu et al. [65], which relates the efficiency to the compressor's pressure ratio (P_r):

$$\eta_{vol} = 0.95 - 0.0125P_r \tag{3}$$

It is important to note that the use of a screw compressor inherently defines a practical scale for the system, because the compressor's capacity is directly linked to its volumetric displacement and rotational speed. Screw compressors are positive displacement machines suited for moderate volumetric flow rates and pressure ratios, which typically translates to thermal outputs from several tens of kilowatts up to about 1–2 MW, depending on the working fluid's density and the enthalpy lift. Therefore, the present analysis assumes a scale that matches typical industrial screw compressor applications, and the results should not be extrapolated beyond this range without re-evaluating the compressor technology.

Hence the work of the compressor is calculated using equation (4).

$$W_{comp} = \dot{m}(h_{3s} - h_2)/\eta_{is} \tag{4}$$

Where $\dot{m}$ is the mass flow rate of the working fluid.

2.3.2. Condenser

The HeatX block was used to simulate the condenser as a single-unit heat exchanger, encompassing desuperheating, condensation, and subcooling. This block offers a single degree of freedom, allowing for the adjustment of the degree of subcooling. To ensure precise calculation of the temperature difference at the pinch point, the condenser was segmented into 100 zones. With the design specification tool, the zonal analysis feature (in the HeatX block) of the Aspen Plus software was utilized to set the condensation pressure and the pressurized water at the sink inlet was used to set the minimum pinch point temperature difference of 5 K at beginning of the condensation process (vapor quality equal 1). Equation (5) presents the energy balance for the condenser.

$$\dot{m}(h_3 - h_6) = \dot{m}_{si}\left(h_{si,out} - h_{si,in}\right) \tag{5}$$

Where h_6 is the enthalpy of the fluid at the exit of the condenser, $h_{si,in}$ is the enthalpy of the heat sink inlet, $\dot{m}_{si}$ is the mass flow rate of the supply water and $h_{si,out}$ is the enthalpy of the heat sink exit. The heat transfer in the condenser is calculated using Equation (6). The shell and tube heat exchanger type was selected for all heat exchangers.

$$Q_{cond} = \dot{m}(h_3 - h_6) \tag{6}$$

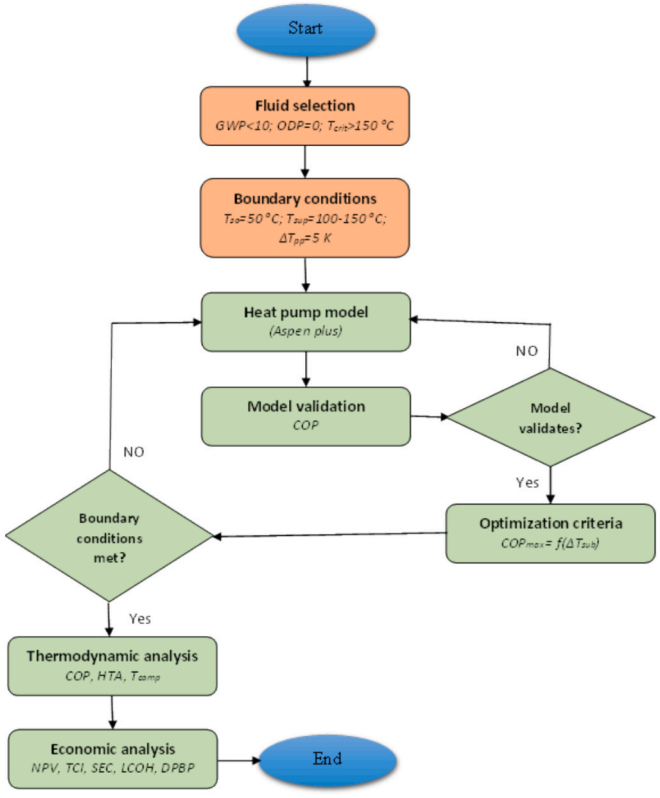

Fig. 3. Simulation flow chat.

2.3.3. Evaporator

The HeatX block was used to model the evaporator, ensuring complete evaporation of the working fluid into the saturated vapor state. A working fluid vapor fraction of 1 was specified at the evaporator outlet in the block. By utilizing the design specification tool, the mass flow rate of the heat source is modified to achieve a heat source exit temperature of 45 °C, at the set evaporation pressure. To enable accurate calculation of the pinch point temperature difference, the evaporator is segmented into 100 zones. Equation (7) provides the energy balance in the evaporator.

$$\dot{m}(h_1 - h_8) = \dot{m}_{so}\left(h_{so,in} - h_{so,out}\right) \tag{7}$$

Where h_1 is the enthalpy of the fluid at the exit of the evaporator, h_8 is the enthalpy of the working fluid at the inlet of the evaporator, $h_{so,in}$ is the enthalpy of the heat source inlet, $\dot{m}_{si}$ is the mass flow rate of the heat source and $h_{so,out}$ is the enthalpy of the heat source exit. The heat transfer in the evaporator is calculated using Equation (8).

$$Q_{eva} = \dot{m}(h_1 - h_8) \tag{8}$$

2.3.4. Internal heat exchanger (IHX)

The HeatX block model is used to simulate the internal heat exchanger (IHX) and meet the cycle's superheat requirements with the heat from the working fluid at the condenser outlet. The term refers to the level of superheating that will prevent any form of liquid phase in the compression process and it is related to the positive slope of the saturated vapor line. Fluids with infinitely large slope in the saturation vapor curve (isentropic fluids), will require less superheat compared to fluids with negative slope in the saturated vapor curve (dry fluids). The compressor block in Aspen Plus is enabled to perform vapor–liquid test to ensure the elimination of any form of wet compression in the compression process. The IHX is modelled in principle analogous to the HEX described above. Equation (9) describes the energy balance in the IHX.

$$(h_2 - h_1) = (h_6 - h_7) \tag{9}$$

Where h_7 is the enthalpy of the working fluid at the inlet of the expansion valve. The heat transferred in the IHX is calculated using equation (10).

$$Q_{IHX} = \dot{m}(h_2 - h_1) \tag{10}$$

2.3.5. Expansion valve

The expansion valve is designed to handle the cycle's expansion requirement in an isenthalpic manner through the valve block. With one degree of freedom, the outlet pressure is specified in the valve block. Utilizing the design specification tool, the pressure was adjusted to achieve a 5 K temperature difference at the evaporator for the cycle. Equation (11) provides the energy balance at the expansion valve.

$$h_7 = h_8 \tag{11}$$

2.4. System performance and optimization

The coefficient of performance (COP) of the system was optimized for the specified boundary conditions, using the optimization feature of the Aspen plus 12.1 simulation software. The optimization tool is composed of four main sections: variable definition, objective, constraints, and variable manipulator. Variable definition specifies the variable(s) used in a Fortran programming language to create the objective function. Only output variables, such as stream or block variables, can be defined. For this study, the calculated compressor work (W_{comp}) and the condenser heat transfer rate ($\dot{Q}_{cond}$) were defined, and the coefficient of performance, which serves as the objective function, was then computed using Equation (12).

$$COP = \dot{Q}_{cond}/W_{comp} \tag{12}$$

The optimization constraint restricts the compressor suction temperature to 80 °C, in line with the recommended safe limit for existing compressors provided by [66]. This limitation results in a superheat degree of 40 K under the specified boundary conditions. As a result of the 5 K pinch point temperature difference in the heat exchangers, it is anticipated that the working fluids will be entirely subcooled, with this minimum pinch point temperature difference applied at the exit of the condenser. Thus the optimisation of the was obtained by varying the evaporation and condensation pressure of the working fluid and maximising the subcooling process in the condenser as considered in [20].

2.5. Heat transfer area calculation

All heat exchangers were modelled as the shell and tube heat exchanger due to the high pressures and temperatures associated with the cycle. Also, the need for pressure drop estimation arises due to its effect on the overall performance of the system. The corresponding calculation methods concerning heat transfer area and pressure drop are described in detail in the following subchapters.

In this study, the working fluid is assigned to the tube side for both condensation and evaporation primarily to ensure consistent and comparable heat exchanger sizing across different working fluids. This approach simplifies the thermal–hydraulic modeling by allowing the use of well-established correlations for two-phase flow inside tubes, which improves the reliability of heat transfer predictions. Furthermore, it provides a clear high-pressure boundary that can be conservatively assessed for safety. While industrial high-temperature heat pumps typically use shell-side condensation to handle larger volumetric flows and facilitate maintenance, the tube-side arrangement used here offers a practical basis for comparative techno-economic screening. This simplification does not affect the validity of the relative trends reported and will be refined in future detailed engineering design stages.

The heat transfer area of the heat exchanger is given by Equation (13).

$$A = \sum_{i}^{n} \dot{Q}_i/(\Delta T.U)_i \tag{13}$$

Where U is the overall heat transfer coefficient, $\dot{Q}$ is the rate of heat transfer, and ΔT is the logarithmic temperature difference. The logarithmic temperature difference is calculated using equation (14).

$$\Delta T = \left[\left(T_{h,in} - T_{c,out}\right) - \left(T_{h,out} - T_{c,in}\right)\right]/\ln\left[\left(T_{h,in} - T_{c,out}\right)/\left(T_{h,out} - T_{c,in}\right)\right] \tag{14}$$

Where the subscripts *h, in, c,* and *out* stand for hot, inlet, cold, and outlet respectively.

2.5.1. Condenser heat transfer area

The heat transfer area (HTA) of the condenser was calculated using Equation (15) to cover for the HTA required for the desuperheating (A_{des}), condensation ($A^{(i)}_{2p.con}$) and subcooling processes (A_{sub}).

$$\begin{aligned} A_{cond} &= \sum_{i=1}^{n} A^{(i)}_{2p.con} + A_{sub} + A_{des} \\ &= \sum_{i=1}^{n} \left(\frac{\dot{Q}^{(i)}_{2p.con}}{\Delta T^{(i)}_{2p.con} U^{(i)}_{2p.con}} \right) + \frac{\dot{Q}_{sub}}{\Delta T_{sub} U_{sub}} + \frac{\dot{Q}_{des}}{\Delta T_{des} U_{des}} \end{aligned} \tag{15}$$

Where $\dot{Q}$ and U are the heat transfer rate and overall heat transfer coefficient respectively. The overall heat transfer coefficient for the condensation, subcooling, and desuperheating processes are calculated using Equation (16), Equation (17), and Equation (18) respectively.

$$\frac{1}{U^{(i)}_{2p.con}} = \frac{d_o/d_i}{h^{(i)}_{2p.con}} + \frac{d_o \ln(d_o/d_i)}{2\lambda_m} + \frac{1}{h_{cw}} \tag{16}$$

$$\frac{1}{U_{sub}} = \frac{d_o/d_i}{h_{sub}} + \frac{d_o \ln(d_o/d_i)}{2\lambda_m} + \frac{1}{h_{cw}} \tag{17}$$

$$\frac{1}{U_{des}} = \frac{d_o/d_i}{h_{des}} + \frac{d_o \ln(d_o/d_i)}{2\lambda_m} + \frac{1}{h_{cw}} \tag{18}$$

Where d_o is the outer diameter of the tube, d_i is the inner diameter of the tube, λ_m is the thermal conductivity of the tube material, h_{cw} is the single-phase heat transfer coefficient of the supply water on the shell side, h_{des} is the single-phase in-tube heat transfer of the working fluid for the desuperheating process, h_{sub} is the in-tube single-phase heat transfer coefficient of the working fluid for the subcooling process and $h^{(i)}_{2p.con}$ is the two phase in tube heat transfer coefficient of the working fluid for the condensation process. The heat transfer coefficient for the two-phase condensation process in the tube side of the condenser was calculated using the correlation of shah [67], as presented in Equation (19).

$$h_{2p.con} = 0.023 Re_{LT}^{0.8} Pr_f^{o.4} \left[(1-x)^{0.8} + \frac{3.8 x^{0.76} (1-x)^{0.04}}{\dot{P}r^{0.38}} \right] \tag{19}$$

The heat transfer coefficient for the single-phase subcooling and desuperheating processes, were calculated using the correlation by Petukhov [68] as presented in Equation (20).

$$h_{sp} = \frac{(f/8) RePr}{K_1(f) + K_2(Pr)\left(f/8\right)^{\frac{1}{2}}\left(Pr^{\frac{2}{3}} - 1\right)} \tag{20}$$

For the single-phase heat transfer coefficient on the shell side, the correlation of Kern [69] was employed as presented in Equation (21).

$$h_{cw} = 0.36 Re^{0.55} Pr^{0.33} \tag{21}$$

2.5.2. Evaporator heat transfer area

The evaporator only took care of the two-phase evaporation process of the working fluid. The HTA of the evaporator was calculated using Equation (22).

$$A_{eva} = \sum_{i=1}^{n} A^{(i)}_{2p.eva} = \sum_{i=1}^{n} \left(\frac{\dot{Q}^{(i)}_{2p.eva}}{\Delta T^{(i)}_{2p.eva} U^{(i)}_{2p.eva}} \right) \tag{22}$$

The overall heat transfer coefficient was calculated using Equation (23).

$$\frac{1}{U^{(i)}_{2p.eva}} = \frac{d_o/d_i}{h^{(i)}_{2p.eva}} + \frac{d_o \ln(d_o/d_i)}{2\lambda_m} + \frac{1}{h_{hw}} \tag{23}$$

The two-phase heat transfer coefficient for evaporation on the tube side was calculated using the correlation of Gungor and Winterton [70] as presented in Equation (24).

$$h_{2p.eva} = E \times h_{sp.f} + h_{NB} + h_{CB} \tag{24}$$

Where E is the convection two-phase multiplier, which is equal to 1 for vertical flows, $h_{sp.f}$ is the liquid single-phase heat transfer coefficient, h_{NB} is the nucleate boiling component of two-phase heat transfer coefficient, and h_{CB} is the convective component of two-phase heat transfer coefficient. $h_{sp.f}$, h_{NB} and h_{CB} were calculated with the combination of Equation (25), Equation (26) and Equation (27).

$$\frac{h_{NB}}{h_{sp.f}} = 3000 E B_o^{0.86} \tag{25}$$

$$h_{CB}/h_{sp.f} = 1.12 E (x_e/1 - x_e) \times 0.75 \left(\rho_f/\rho_g\right)^{0.41} \tag{26}$$

$$h_{sp.f} = 0.023 Re_{f.D}^{0.8} Pr_f^{0.4} \frac{K_f}{D} \tag{27}$$

Where B_o is the boiling number, x_e is the thermodynamic equilibrium quality of the working fluid, ρ is the density, $Re_{f.D}$ is the liquid Reynolds number based on tube diameter, Pr_f is the Prandtl number at saturated conditions, K_f is the thermal conductivity of liquid at saturated condition, and D is the tube inner diameter.

2.5.3. Internal heat exchanger heat transfer area

The heat transfer area of the IHX was calculated using Equation (28).

$$A_{IHX} = \frac{\dot{Q}_{IHX}}{\Delta T_{IHX} U_{IHX}} \tag{28}$$

The overall heat transfer coefficient of the IHX is calculated using Equation (29).

$$1/U_{sub} = \frac{d_o/d_i}{h_{tub}} + \frac{d_o \ln(d_o/d_i)}{2\lambda_m} + \frac{1}{h_{sh}} \tag{29}$$

The heat transfer coefficient of the shell (h_{sh}) and tube (h_{tub}) sides were calculated using Equation (21) and Equation (30).

$$h_{tub} = 0.027 Re^{0.8} Pr^{0.33} \tag{30}$$

2.5.4. Pressure drop estimation

The pressure drops In the heat exchangers were estimated using the expressions suggested by Peters et al. [71] on the shell side and Uday and Satish [72] on the tube side, for shell and tube heat exchanger type. These expressions were fitted into the respective heat exchanger models using the calculator block provided in the software.

The expressions pressure drops are presented in Table 5.

2.6. Economic model

The system cost of a heat pump can be estimated through direct market surveys or by using cost functions [13]. Cost estimation methods are more convenient and easier to use but may yield results that deviate somewhat from direct market surveys. While current costs can be obtained from market surveys, results from cost functions need to be adjusted to recent periods using the equipment index of Chemical Engineering Plant Cost Index (CEPCI) [73]. These deviations arise from specific details such as operating pressure factors and component construction materials. The cost functions provide estimates for the cost of components, operation, and overall system investment [13]. In component cost estimation, the specific capacity parameters of the components, such as heat duty or heat transfer area [74–76] for heat exchangers and power, isentropic efficiency, displacement volume, and pressure ratio [74,75,77–79] for compressors, play a significant role. The cost estimation developed by Smith [80] from 2005 was adopted for this study. The corresponding CEPCI of 468 was set in relation to the value of January 2024 with 803, to accommodate the inflation in the prices of raw materials, personnel cost and production processes.

The annual revenue was considered constant throughout the lifetime

Table 5
Isentropic efficiency and pressure drop correlation.

Parameters	Correlations	Reference
Pressure drop (tube side)	$\Delta P_t = \Delta P_i + \Delta P_o + \Delta P_{tubes} + \Delta P_c$	Uday and Satish [72]
Pressure drop (shell side)	$\Delta P_{shell} = \frac{2fG_s^2 D_s (N_B + 1)}{\rho D_e \left[\frac{\mu}{\mu_s}\right]^{0.14}}$	Peters et al. [71]

of the plant and calculated using Equation (31) as the product of the cost of heat supply (C_{heat}), the capacity of the plant ($\dot{Q}$), and the yearly operating hours (N).

$$REV_i = C_{heat}.\dot{Q}.N \tag{31}$$

The discounted payback period was calculated using Equation (32). Where $F_{o\&M}$ is the plant operation and maintenance factor, TCI is the total investment cost, and I_r is the interest rate. The operation and maintenance factor and interest rate of 90 % and 5 % respectively, typical for waste recovery [81], were used. All the cost parameters are summarized in Table 3 Table 6.

$$DPBP = \frac{\ln\left(\frac{F_{o\&M}.REV_i}{F_{o\&M}.REV_i - I_r.TCI}\right)}{\ln(1+I_r)} \tag{32}$$

The project cost, known as the total investment cost, encompasses all expenses related to establishing and operating the plant. In addition to equipment and auxiliary costs, it includes labor, overhead, construction, and integration costs for the heat recovery project. The calculation involved applying a multiplication factor of 4.16 to the purchased equipment cost (TEC) [19], as outlined in Equation (33). The specific investment cost (SIC) of the entire heat pump system is determined by dividing TCI by the heating capacity.

$$TCI = 4.16TEC \tag{33}$$

The total equipment cost (TEC) is the sum of the cost of the main components and the auxiliary cost (C_{aux}), as presented in Equation (34). The specific equipment cost (SEC) is calculated as the division of TEC by the heating capacity.

$$TEC = C_{com} + C_{cond} + C_{eva} + C_{IHX} + C_{aux} \tag{34}$$

The auxiliary cost accounts for the costs of piping and tanks (including oil circuits, valves, and fittings) as well as electrical equipment (including control panels, switches, and electronic expansion valve). It is expressed as 20 % of the sum of the cost of the base equipment [19], as presented in Equation (35).

$$C_{aux} = 0.20(C_{com} + C_{cond} + C_{eva} + C_{IHX}) \tag{35}$$

The determination of the feasibility of the studied working fluids utilizes the levelized cost of heat (LCOH), which is a key economic parameter. LCOH is calculated based on the total investment cost, auxiliary expenses, and the cost recovery factor (CRF) outlined in Equation (36).

$$LCOH = \left(CRF \times TCI + C_{aux} + [C_{elec} \times H_{cap} \times L_t \times N]\right)/\left(N \times H_{cap} \times L_t \times COP\right) \tag{36}$$

To estimate the purchase equipment cost of the main components, the component cost according to Smith [80]. This equipment cost model calculates the cost of heat exchangers and compressor as a function of heat transfer area and power respectively using Equations (37) and (38).

Table 6
Cost estimation assumptions.

Parameters	Values
Yearly operating hours (N)	7000 h
HTHP capacity ($\dot{Q}$)	1000 kW
Cost of electricity (C_{elec})	0.192 €/kWh[82]
Cost of heat supply (C_{heat})	0.142 €/kWh[82]
Lifetime of system (L_t)	20 years
Interest rate (I_r)	5 %
Euro conversion ratio	0.95 €/$

$$C_{hx} = 32800\left(\frac{A}{80}\right)^{0.68} \tag{37}$$

$$C_{comp} = 98400\left(\frac{P}{250}\right)^{0.46} \tag{38}$$

The compressor cost model includes the cost of the motor. The heat exchanger in this case is the shell and tube heat exchanger. The boundary conditions for the cost models are summarized in Table 7

2.7. Verification of thermodynamic model

The verification of the model in this study was based on the experimental results for a high-temperature heat pump system using R1233zd (E) as working fluid of Jeßberger et al. [25]. As reference case of 60 °C for the heat source and 140 °C for the sink temperatures are considered. The isentropic efficiency of the compressor is estimated by the model of Astolfi et al. [64] for this validation. The pressure-drop correlations for the heat exchangers adopted for this investigation were also applied in this validation. The model was verified in respect to COP, displayed in Fig. 4. The observed COP variations for all scenarios were just around the 10 % range, indicating good cycle prediction by the developed model. These variations may be attributed to unaccounted energy losses in the model.

3. Results and discussion

3.1. Thermodynamic performance

3.1.1. Coefficient of performance (COP)

Fig. 5 shows that the COP of all six working fluids decreases consistently with increasing supply temperature, a trend widely supported by findings in literature [37,43,83] due to higher compression work and reduced thermodynamic efficiency at elevated temperatures. Cyclopentane consistently delivers the highest COP, outperforming hexane by up to 15 % at 150 °C, owing to its favorable critical properties and higher isentropic efficiency. In contrast, hexane and cyclohexane exhibit the lowest COPs (2.42 and 2.50 at 150 °C, respectively), primarily due to reduced compressor isentropic efficiency—below 0.5 for hexane at high temperatures. These results align with prior studies showing cyclopentane's strong performance in high-temperature applications, while heavier alkanes like hexane underperform due to poor compression characteristics. These results strengthen the conclusions that fluids with superior compressor efficiency and suitable critical properties are optimal for high-temperature heat pump cycles Fig. 6.

3.1.2. Compressor discharge temperature

The highest temperature within a vapor compression cycle typically occurs at the compressor outlet [84], making it a critical parameter due to its influence on compressor reliability, lubricant stability, and material durability [85]. Fig. 7 illustrates the compressor discharge temperatures for the six working fluids at various supply temperatures, revealing marked variations in thermal behavior. Cyclic hydrocarbons such as cyclopentane and cyclohexane exhibit significantly higher discharge temperatures, reaching up to approximately 200 °C at a supply temperature of 150 °C. This is nearly 27 °C higher than that of

Table 7
Cost model equipment capacity limit.

Models	Components	Capacity	Unit	min	max
Smith [80]	Compressor (including motor)	Power	kW	250	1000
	Heat exchanger (shell and tube)	Heat transfer area	m^2	80	400

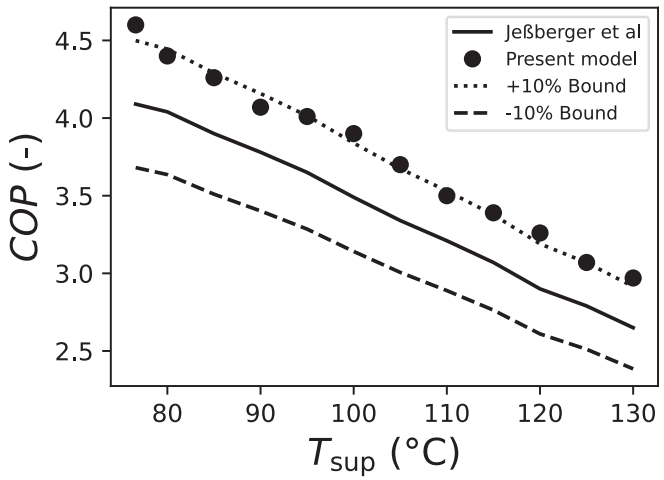

Fig. 4. Comparison of the COP obtained from the present model to that of Jaromir et al. [25] at various supply temperature.

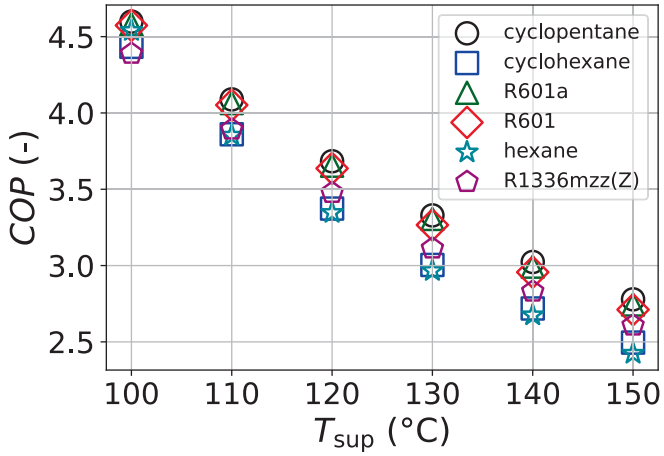

Fig. 5. COP comparison of different supply temperatures.

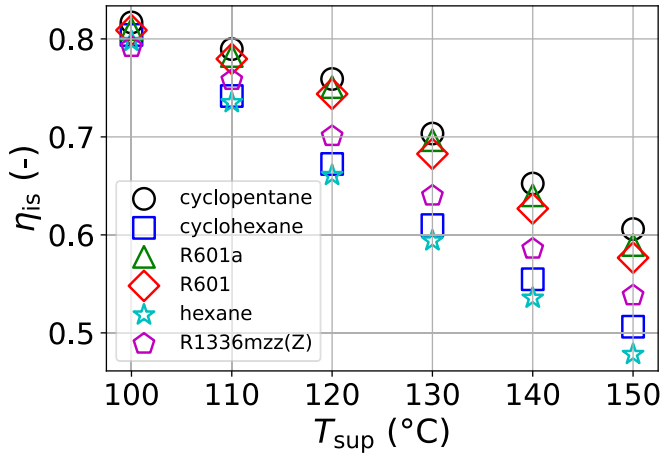

Fig. 6. Isentropic efficiency at different supply temperatures.

R601a, which registers the lowest discharge temperature among the fluids evaluated. The elevated discharge temperatures associated with cyclic hydrocarbons are attributed to their higher specific heat ratios and reduced isentropic efficiency at elevated temperatures, which result in greater temperature rises during compression. These high discharge

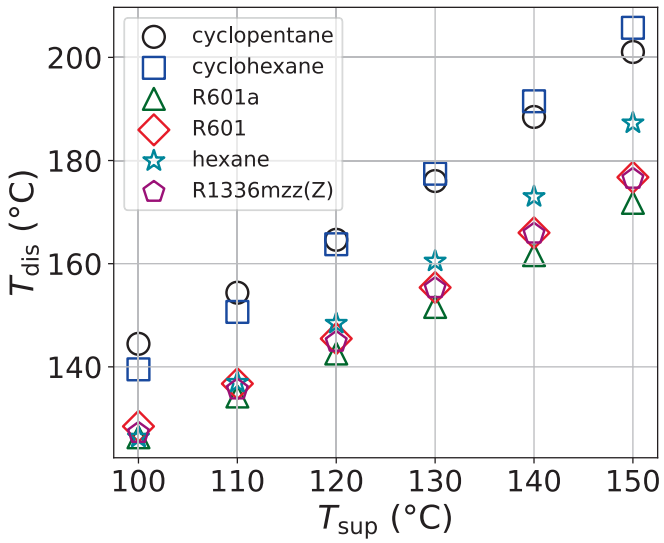

Fig. 7. Compressor discharge temperatures at different supply temperatures.

temperatures exceed the recommended thermal limit of 180 °C for polyol ester (POE) compressor lubricants [66,86], thereby raising concerns regarding lubricant degradation and potential compressor failure. In contrast, linear hydrocarbons like hexane and R601a maintain lower discharge temperatures under the same conditions, with hexane staying just above the lubricant threshold at a supply temperature of 150 °C. Consequently, despite its lower COP, hexane presents a thermally safer option for high-temperature applications in ORC systems, particularly where long-term compressor performance and oil stability are critical. This emphasizes the importance of balancing thermal efficiency with mechanical and chemical durability in the selection of working fluids.

3.1.3. *Mass flow rate of working fluid*

Fig. 8 reveals that the synthetic working fluid R1336mzz(Z) consistently demonstrates the highest mass flow rate across the full range of supply temperatures studied. This trend aligns with existing literature, which attributes the elevated mass flow rates of synthetic fluids to their relatively low enthalpy of evaporation [87]. In contrast, the organic fluids typically used in Organic Rankine Cycle (ORC) systems—such as cyclohexane, R601a, and other hydrocarbons—exhibit much lower mass flow rates due to their higher latent heat of vaporization. This allows a smaller quantity of fluid to transfer the same amount of heat, which not only improves system compactness but also reduces the required working fluid charge and associated material costs. Among the ORC

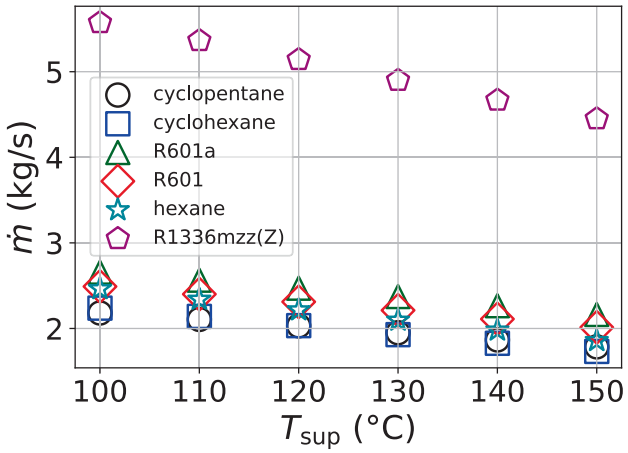

Fig. 8. Mass flow rate comparison at various supply temperatures.

fluids examined, cyclohexane stands out with the lowest mass flow rate at all tested supply temperatures. Quantitatively, its mass flow rate is approximately 150 % lower than that of R1336mzz(Z), and about 18 % lower than R601a. This substantial reduction in flow rate translates into smaller equipment sizing for pumps and heat exchangers, lower pumping power, and reduced environmental and economic impact from working fluid losses or leaks. Consequently, while synthetic fluids like R1336mzz(Z) may offer some thermodynamic benefits, the significantly higher mass flow rates demand careful consideration of equipment design, operating costs, and fluid handling systems, especially in large-scale or long-duration applications.

3.1.4. Condenser heat transfer area

The heat transfer area (HTA) is a critical parameter governing the capital cost of heat exchanger equipment, as a larger HTA directly implies greater material usage, fabrication complexity, and associated expenditures. Fig. 9 illustrates the variation of the condenser HTA for the working fluids under study as a function of the supply temperature. As shown, the condenser HTA systematically decreases with increasing supply temperature—a trend that aligns with thermodynamic principles. This behaviour can be attributed primarily to the increasing temperature glide within the condenser at higher supply temperatures, which enhances the mean temperature difference between the condensing vapor and the cooling medium. Consequently, a larger driving force for heat transfer is established, allowing the required duty to be achieved with a smaller heat exchange surface.

The magnitude of the HTA requirement also varies considerably among the different working fluids employed in the ORC systems. This variation stems from differences in thermophysical properties such as latent heat of vaporization, specific heat capacity, and the degree of temperature glide during phase change. For instance, across the examined supply temperature range, the disparity in condenser HTA can reach up to 50 % between fluids such as cyclohexane and R1336mzz(Z). Notably, cyclohexane requires a substantially larger HTA due to its relatively lower temperature glide and different condensation characteristics, which result in a lower average temperature difference and therefore demand a greater surface area to achieve the same heat duty.

3.1.5. Internal heat exchanger heat transfer surface area

Fig. 10 illustrates the variation in the internal heat exchanger (IHX) heat transfer surface area for the selected working fluids across the range of supply temperatures investigated. Among the working fluids considered, cyclohexane and hexane exhibit consistently higher IHX heat transfer areas at all supply temperatures, with the maximum difference reaching approximately 60 % compared to R1336mzz(Z). This

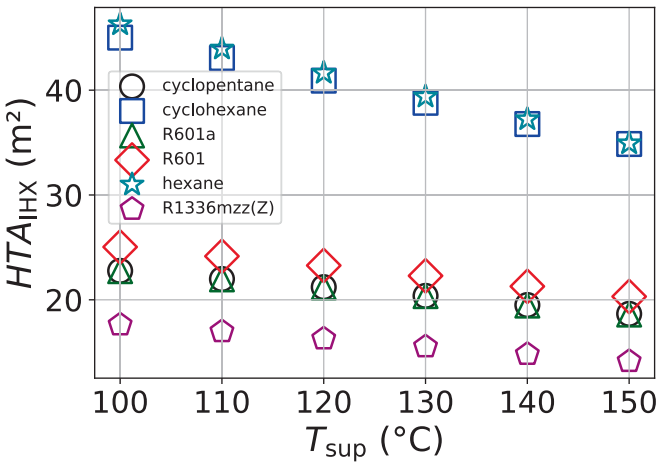

Fig. 10. Internal heat exchanger heat transfer area for different fluids as a function of supply temperature.

significant disparity arises primarily from their thermodynamic behaviour and the greater degree of superheating required to mitigate the risk of wet compression during expansion. In contrast, cyclopentane demonstrates a more moderate IHX surface area requirement throughout the supply temperature range, with deviations of about 25 % relative to R1336mzz(Z). This can be attributed to its favourable thermodynamic characteristics, particularly its relatively steep saturation vapor curve, which results in near-isentropic expansion behaviour.

Both cyclopentane and R1336mzz(Z) possess more vertically oriented saturation vapor curves compared to other investigated fluids, which reduces the tendency for vapor condensation during expansion. As a result, these fluids require a lower degree of superheating to ensure dry expansion conditions, thereby decreasing the necessary heat transfer duty within the IHX. Consequently, R1336mzz(Z) consistently exhibits the lowest IHX heat transfer surface area among the working fluids studied, highlighting its advantage in reducing heat exchanger size and associated capital costs for ORC systems. This behaviour aligns with observations reported in previous studies [88,89], which demonstrate that working fluids with steeper saturation vapor curves maintain higher vapor quality, minimizing the need for extensive superheating and thus reducing the heat exchanger surface area requirement.

3.1.6. Evaporator heat transfer surface area

Fig. 11 presents the variation in the heat transfer surface area of the evaporator for the selected working fluids across the investigated supply

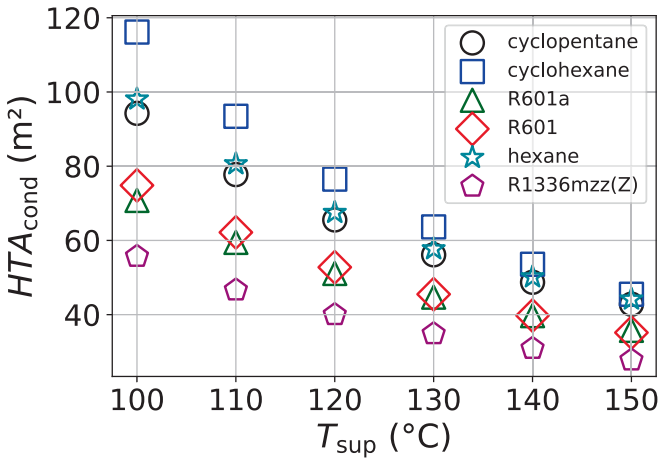

Fig. 9. Condenser heat transfer area for different fluids as a function of supply temperature.

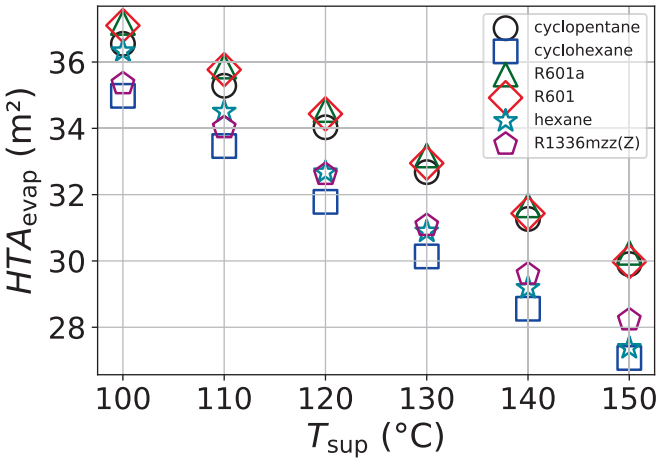

Fig. 11. Evaporator heat transfer area for different fluids as a function of supply temperature.

temperature range. Among the fluids evaluated, the cyclic hydrocarbons—cyclohexane and cyclopentane—demonstrate consistently lower evaporator heat transfer area requirements compared to the other working fluids, with the maximum difference reaching approximately 15 % relative to R601a under lower supply temperature conditions. Notably, this difference becomes more pronounced at elevated supply temperatures, increasing by approximately 12 %, indicating that the performance advantage of the cyclic hydrocarbons in reducing evaporator size is amplified at higher heat source temperatures. The two cyclic hydrocarbons, cyclohexane and cyclopentane, exhibit nearly identical evaporator heat transfer areas across the entire supply temperature range investigated, with deviations within only 0.3 %. This similarity can be attributed to their comparable thermophysical properties, including latent heat of vaporization and saturation curve characteristics, which govern phase change behaviour and heat transfer performance in the evaporator.

In general, the required evaporator heat transfer area decreases as the supply temperature increases. This trend is primarily due to the higher vapor fraction achieved at the evaporator outlet under elevated supply temperatures, which increases the mean temperature difference between the heat source and the working fluid during phase change. The resulting higher thermal driving force reduces the surface area required to achieve the desired heat duty. Additionally, a higher supply temperature typically shifts the working fluid closer to its saturation temperature at the evaporator inlet, thereby shortening the sensible heating region and enhancing the overall heat transfer effectiveness.

A summary of the thermodynamic performance indicators for the various working fluids at 150 °C supply temperature is provided in Table 8.

3.2. Economic performance

3.2.1. Specific equipment cost

Fig. 12 illustrates the variation in specific equipment costs (SEC) for the investigated working fluids across the range of supply temperatures. In general, SEC exhibits an increasing trend with rising supply temperature. This behaviour is primarily driven by the higher pressure ratios required at elevated supply temperatures, which directly translate into increased mechanical and material demands for key system components such as compressors and heat exchangers, thereby elevating overall capital costs [90]. When comparing the organic Rankine cycle (ORC) working fluids to the baseline fluid R1336mzz(Z), cyclohexane and hexane consistently demonstrate higher SEC values throughout the entire supply temperature range, with the maximum deviation reaching approximately 9.1 % at a supply temperature of 150 °C. This discrepancy arises mainly from the higher-pressure ratios required by these linear hydrocarbons at larger temperature lifts, which increase compressor size and associated costs. Conversely, cyclopentane exhibits a more moderate SEC profile, comparable to that of R601 and R601a, with only a slight difference of approximately 1.8 % relative to R1336mzz(Z). This modest difference is attributed to cyclopentane's favourable thermodynamic characteristics, including a steeper saturation vapor curve and lower required superheat, which collectively reduce the compression work and associated equipment costs.

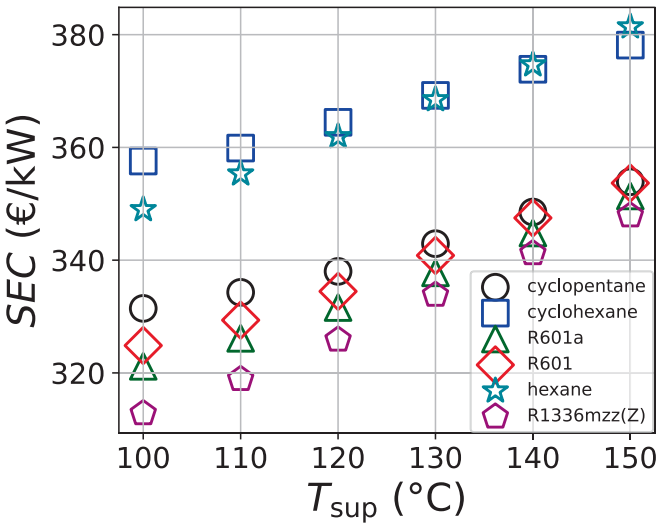

Fig. 12. Specific equipment cost as a function of supply temperature.

Fig. 13 provides a detailed breakdown of the contributions of individual system components to the overall SEC for cyclopentane at supply temperatures of 100 °C and 150 °C. The compressor emerges as the dominant cost driver, accounting for 62.1 % of the total SEC at a supply temperature of 100 °C, and rising substantially to 74.6 % at 150 °C. This increase reflects the greater work input and mechanical design requirements necessary to achieve the higher-pressure ratio and temperature lift at elevated supply temperatures. In contrast, the contributions from the evaporator and the internal heat exchanger (IHX) decrease as the supply temperature rises. Notably, while the IHX remains the smallest contributor to total SEC at both temperature levels, the evaporator's contribution shifts from the second-largest component at 100 °C to the third largest at 150 °C. This reordering aligns with the observed reduction in evaporator heat transfer area requirements at higher supply temperatures, as well as with the findings reported by [19], which highlight the dominant role of the compression process in driving HTHP system costs under conditions of significant temperature lift.

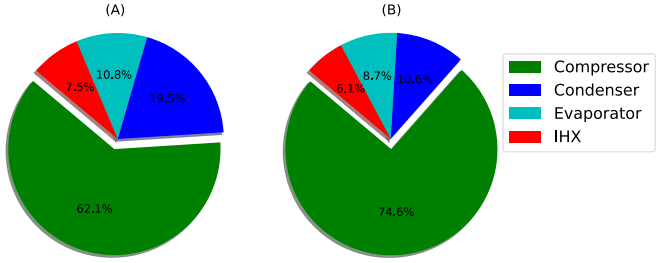

Fig. 13. Percentage bare module cost contribution of the components for cyclopentane; (a) 100 °C supply temperature (b) 150 °C supply temperature.

Table 8
Performance index at 150 °C supply temperature.

Parameters	Working fluids					
	Cyclohexane	Cyclopentane	Hexane	R601	R601a	R1336mzz(Z)
COP (–)	2.50	2.79	2.42	2.71	2.75	2.61
Evaporator pressure (bar)	0.23	0.71	0.37	1.16	1.52	1.21
Condensing pressure (bar)	3.44	8.01	4.98	11.74	14.20	13.31
Condenser HTA (m^2)	45.50	42.81	44.15	35.16	35.77	27.77
Evaporator HTA (m^2)	27.07	29.90	27.38	29.98	30.24	28.23
IHX HTA (m^2)	34.86	18.66	34.93	20.31	18.59	14.13
Mass flowrate (kg/s)	1.73	1.79	1.86	2.01	2.16	4.45

3.2.2. Specific investment cost (SIC)

Fig. 14 presents the specific investment cost (SIC) of the entire high-temperature heat pump system as a function of varying cost factors for the different working fluids at a supply temperature of 150 °C. As anticipated, the SIC exhibits a positive correlation with increasing cost factors, with a 30 % rise in the cost factor resulting in an approximate 37 % increase in the overall SIC. This proportional increase reflects the direct impact of material, fabrication, and installation cost escalations on the capital expenditure of the heat pump system. Among the working fluids examined, cyclohexane and hexane consistently yield the highest SIC values across the entire cost factor range, with a maximum deviation of approximately 8 % compared to R1336mzz(Z) at a supply temperature of 150 °C. This elevated investment cost is primarily attributed to their higher required heat transfer areas and greater compressor costs, resulting from less favourable thermodynamic properties such as broader temperature glides and higher-pressure ratios at elevated supply temperatures.

In contrast, cyclopentane demonstrates SIC values that remain well within the range of those observed for R601 and R601a. At a supply temperature of 150 °C, the SIC for cyclopentane differs by only about 1.8 % relative to R1336mzz(Z). This modest variation highlights cyclopentane's competitive performance from an economic standpoint, which can be attributed to its advantageous thermo-physical properties—specifically, its steep saturation vapor curve and lower superheat requirement, which help minimize compressor and heat exchanger costs. Overall, these findings indicate that cyclopentane is a viable alternative to conventional high-temperature heat pump working fluids, offering comparable investment costs while maintaining favourable thermodynamic performance. This economic competitiveness, combined with its moderate specific equipment costs and manageable heat exchanger requirements, reinforces cyclopentane's suitability for advanced ORC and high-temperature heat pump applications.

3.2.3. Discounted payback period

The discounted payback period (DPBP) is a widely applied metric for evaluating the economic viability and liquidity of capital-intensive projects such as high-temperature heat pumps (HTHPs) and organic Rankine cycle (ORC) systems. Unlike the simple payback period, the DPBP incorporates the time value of money by discounting future cash inflows, thereby providing a more realistic estimate of the time required for the cumulative discounted cash flows to recover the initial capital investment [19,73]. This makes it a preferred indicator for techno-economic analyses of energy conversion systems where long operational lifetimes and fluctuating energy prices are relevant considerations.

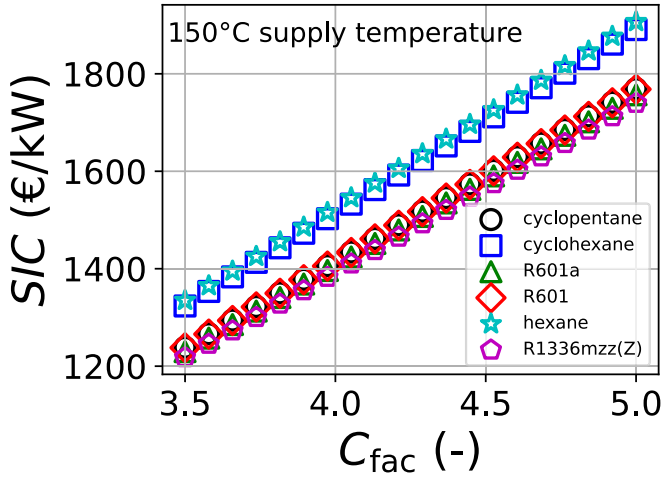

Fig. 14. Specific investment cost as a function of cost factor at 150 °C supply temperature.

Fig. 15 illustrates the variation in DPBP for the HTHP system utilizing different working fluids, evaluated over a range of heat and electricity prices. The results indicate that the DPBP decreases with increasing heat cost, as higher revenues from heat supply accelerate the recovery of the initial investment. Conversely, the DPBP increases with rising electricity costs, as higher operating expenses reduce net cash inflows, thereby extending the payback period. This observed behaviour aligns well with findings reported in previous studies [39], confirming the significant influence of energy price dynamics on the economic performance of thermally driven systems. Among the fluids studied, cyclohexane and hexane consistently exhibit higher DPBP values relative to R1336mzz(Z), with a maximum deviation of approximately 8.7 % at a supply temperature of 150 °C. This can be attributed to their higher specific investment costs, driven by larger heat exchanger areas and increased compressor power requirements, which elevate both capital and operating costs.

In contrast, cyclopentane demonstrates moderate DPBP values that remain close to those of R1336mzz(Z). At a supply temperature of 150 °C, the difference between cyclopentane and R1336mzz(Z) is only about 1.9 %, indicating that cyclopentane maintains competitive payback performance. This is largely due to its favourable thermodynamic behaviour, which results in more efficient system operation and moderate equipment costs. Furthermore, sensitivity analysis reveals that under scenarios of elevated electricity prices combined with reduced heat selling prices, the DPBP for cyclohexane and hexane increases more significantly than for other fluids. This underscores their higher sensitivity to operating cost fluctuations, which can further disadvantage their economic feasibility in markets with volatile electricity prices.

3.2.4. Net Present Value (NPV)

The net present value (NPV) is a fundamental indicator for evaluating the overall economic viability and profitability of capital-intensive projects such as high-temperature heat pump (HTHP) systems. Unlike the discounted payback period (DPBP), which only assesses the time required to recover the initial investment, the NPV accounts for the totality of discounted cash flows generated over the entire project lifetime, thereby providing a comprehensive measure of a project's net financial benefit. A positive NPV indicates that the project is expected to generate net economic gains, while a negative NPV implies that the investment would lead to a financial loss.

Fig. 16 illustrates the variation in NPV for the HTHP system employing different working fluids under varying heat and electricity cost scenarios. The results demonstrate that the NPV remains positive across all working fluids and supply temperatures investigated, confirming the economic feasibility of the system configurations within the assumed economic framework. As expected, the NPV exhibits a positive correlation with increasing heat selling prices, due to higher revenue streams, and a negative correlation with rising electricity prices, owing to increased operational expenditures that erode net profit margins. This trend is consistent with observations reported in the literature for ORC and HTHP systems operating under fluctuating energy market conditions. The differences in NPV among the working fluids become more pronounced under scenarios of elevated electricity prices. Cyclohexane and hexane consistently yield lower NPV values compared to R1336mzz (Z), with deviations reaching up to 4.5 %. This reduction can be attributed to the higher specific investment costs and increased compression energy demands associated with these fluids, which amplify sensitivity to electricity price fluctuations and operating costs.

In contrast, cyclopentane exhibits NPV values comparable to those of R601 and R601a, with only a marginal deviation of approximately 3 % relative to R1336mzz(Z). This indicates that cyclopentane maintains robust economic performance across different heat and electricity price scenarios. Its favourable thermodynamic properties—such as lower superheat requirements and more efficient compression—help contain capital and operational costs, thereby sustaining higher net profitability over the project lifetime. Overall, these findings highlight that while all

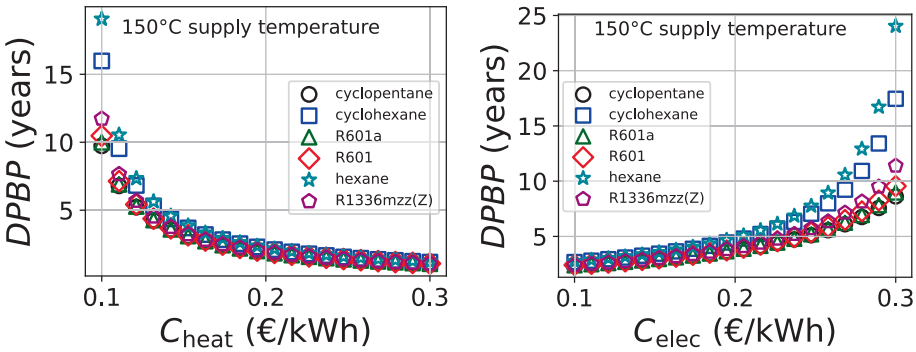

Fig. 15. Discounted payback period as a function of heat and electricity costs.

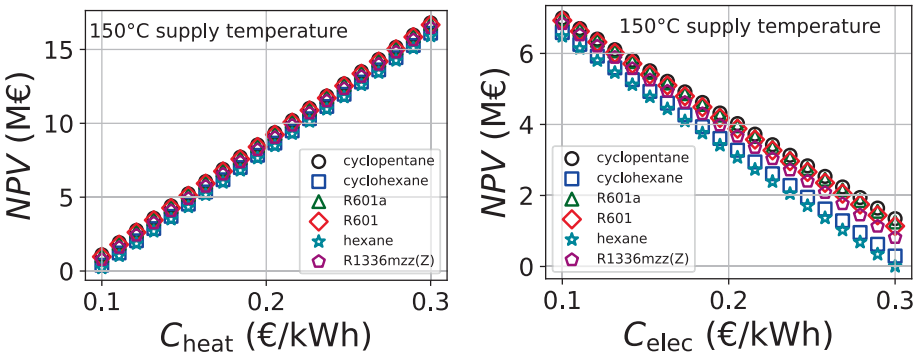

Fig. 16. Net present value as a function of heat and electricity costs.

working fluids analysed can achieve positive NPV under the given conditions, the choice of working fluid significantly influences the sensitivity of the investment's profitability to energy price fluctuations. This emphasizes the importance of careful working fluid selection when optimizing HTHP systems for long-term economic sustainability.

3.2.5. *Levelized cost of heat (LCOH)*

Fig. 17 depicts the variation in the levelized cost of heat (LCOH) for the high-temperature heat pump (HTHP) system employing different working fluids under a range of electricity price scenarios. The LCOH is a key techno-economic performance metric that represents the average cost per unit of useful thermal energy delivered by the system over its operational lifetime, accounting for capital expenditure, operation and maintenance costs, and energy costs, normalized by the total thermal output. The results indicate that the LCOH increases with rising electricity prices, primarily due to the greater share of electrical input required to achieve and maintain higher supply temperatures in the HTHP cycle. Elevated electricity prices directly raise the operational costs associated with compressor work and auxiliary systems, thereby driving up the LCOH. This trend aligns with the thermodynamic behaviour of high-temperature cycles, where higher supply temperatures generally lead to higher pressure ratios and, consequently, greater electrical energy consumption for compression.

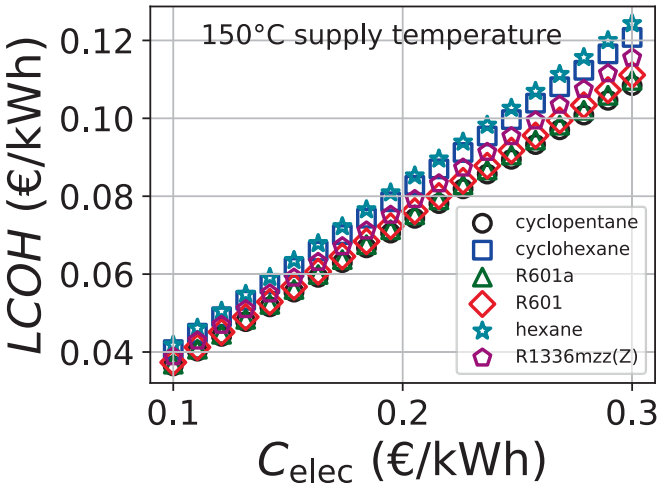

Fig. 17. Levelized cost of heat as a function of supply temperature.

Among the fluids investigated, cyclohexane and hexane consistently yield higher LCOH values relative to the other working fluids. This can be attributed to their higher specific investment costs and increased compressor power requirements, resulting from less favourable thermophysical properties such as wider temperature glides and higher vaporization enthalpy. In contrast, cyclopentane demonstrates moderate LCOH values that remain comparable to those of conventional low-GWP hydrocarbons, such as pentane (R601) and isopentane (R601a). This reflects its more advantageous thermodynamic characteristics—namely, a steeper saturation vapor curve and lower required superheat—which enable efficient heat transfer and lower compressor energy demands. Overall, the LCOH values obtained in this analysis, ranging from 0.04 to 0.125 €/kWh for the selected working fluids, are consistent with values reported in the literature for comparable high-temperature heat pump and ORC applications [91–93]. These findings reinforce the economic competitiveness of cyclopentane relative to conventional working fluids, highlighting its potential as a technically viable and economically attractive option for sustainable high-temperature thermal energy supply.

4. Conclusion

A comprehensive thermo-economic investigation was conducted to evaluate the feasibility of integrating cyclic hydrocarbons with high critical temperatures as working fluids in high-temperature heat pump

(HTHP) systems. The analysis demonstrates that cyclopentane achieves an enhancement of approximately 7.9 % in the coefficient of performance (COP) relative to the reference fluid R1336mzz(Z) at a supply temperature of 150 °C. However, this improved performance is accompanied by an increase in compressor discharge temperature of approximately 21 °C, which imposes additional thermal stress on the compressor components and places more stringent demands on material selection, manufacturing tolerances, and thermal management within the compression stage.

In contrast, R1336mzz(Z) is constrained to supply temperatures near 150 °C primarily due to its subcritical cycle operation at lower pressures or the need for significant superheating to prevent wet compression, which can limit system efficiency. The elevated discharge temperatures observed for the ORC-derived working fluids present additional operational challenges; for instance, cyclohexane and cyclopentane show respective increases in discharge temperature of approximately 14 % and 12.5 % compared to R601a. These higher discharge temperatures necessitate advanced compressor designs and robust thermal management strategies. Hexane, however, demonstrates comparatively moderate discharge temperatures that remain within the operational limits of conventional reciprocating compressor technologies, rendering it more technically compatible with current compressor design envelopes for supply temperatures up to 150 °C.

From a heat exchanger design perspective, the working fluids originating from ORC applications exhibit a notable increase in condenser heat transfer surface area requirements—up to 53 % higher than the baseline—due to their thermophysical properties and temperature glide characteristics. Conversely, cyclohexane and hexane result in a 14.7 % reduction in evaporator heat transfer area across the entire range of supply temperatures studied, which can partially offset increased capital costs associated with larger condenser sizing.

The economic evaluation revealed that the specific equipment cost (SEC) for cyclohexane and hexane can increase by up to 9.1 % relative to R1336mzz(Z), particularly at elevated supply temperatures where higher pressure ratios and larger heat exchanger areas are required. Cyclopentane, however, demonstrates a minimal increase in SEC—within 2 % compared to R1336mzz(Z)—underscoring its balanced trade-off between thermodynamic performance and capital cost. A similar trend is reflected in the discounted payback period (DPBP), where cyclohexane and hexane exhibit increase of up to 8.7 %, while cyclopentane remains within a 2 % deviation relative to the reference fluid at a supply temperature of 150 °C.

A detailed breakdown of component cost contributions reveals that the compressor is the dominant cost driver for the HTHP system, accounting for up to 74.6 % of total equipment cost for cyclopentane at a 150 °C supply temperature. This highlights the critical need to focus technological improvements on compressor efficiency and materials capable of withstanding elevated discharge temperatures and pressure ratios. The levelized cost of heat (LCOH) computed in this study, ranging from 0.04 to 0.125 €/kWh for the working fluids investigated, aligns well with previously published values by Vieren et al. [92] and Gilbert et al. [91], corroborating the economic competitiveness of these alternative fluids for industrial process heat applications.

While the high critical temperatures of these ORC-derived working fluids offer clear advantages for extending HTHP operating ranges into higher temperature process heat markets, certain thermodynamic and techno-economic trade-offs must be addressed. Specifically, with current reciprocating compressor technologies, the practical upper limit for cyclohexane and cyclopentane is projected to be approximately 140 °C to ensure reliable compressor operation without excessive discharge temperatures. Hexane emerges as the most suitable ORC-derived working fluid among those evaluated, with thermal and operational characteristics that are well-matched to existing compressor capabilities for supply temperatures up to 150 °C.

Overall, cyclopentane demonstrates strong potential for integration into HTHP systems, combining favourable thermodynamic performance (higher COP) with specific equipment costs and economic payback metrics that are competitive with established working fluids. This positions cyclopentane as a promising candidate for advancing the replacement of fossil-fuel-based boilers with high-efficiency, low-carbon heat pump technologies in industrial sectors such as metal processing, paper production, and the chemical industry.

Nevertheless, this study underscores the need for further targeted research to address remaining technical barriers, particularly concerning the compatibility of these ORC-derived working fluids with current compressor technologies, lubricant formulations, and sealing systems capable of withstanding elevated suction and discharge temperatures. In addition, comprehensive life-cycle assessments are recommended to fully quantify the environmental impacts and potential sustainability trade-offs associated with deploying these fluids at scale in industrial high-temperature heat pump applications. A limitation of this study is the simplified assumption that the working fluid is always on the tube side for both evaporation and condensation. This ensures consistent sizing and reliable modelling but does not reflect typical industrial practice, where shell-side phase change is often used to handle larger flows and ease maintenance. Future work should address this by exploring alternative heat exchanger configurations—such as shell-side arrangements, plate, or compact heat exchangers—to refine the techno-economic assessment and better represent real-world system design. Finaly, this study assumes the use of a screw compressor, which inherently defines a practical system scale. Screw compressors are positive displacement machines suited for moderate volumetric flow rates and pressure ratios, typically covering thermal outputs from several tens of kilowatts up to about 1–2 MW, depending on the working fluid and operating conditions. As such, the results are valid within this range and should not be extrapolated to larger or smaller capacities without reassessing the choice of compressor technology.

CRediT authorship contribution statement

Echezona Obika: Writing – review & editing, Writing – original draft, Validation, Methodology, Funding acquisition, Formal analysis, Data curation, Conceptualization. **Florian Heberle:** Writing – review & editing, Validation, Supervision, Conceptualization. **Dieter Brüggemann:** Writing – review & editing, Supervision.

Declaration of competing interest

The authors declare the following financial interests/personal relationships which may be considered as potential competing interests: Echezona Obika reports financial support was provided by German Academic Exchange Service. Echezona Obika reports financial support was provided by Petroleum Technology Development Fund. Echezona Obika reports article publishing charges was provided by German Research Foundation. If there are other authors, they declare that they have no known competing financial interests or personal relationships that could have appeared to influence the work reported in this paper.

Acknowledgement

The authors acknowledge the German Academic Exchange Service (DAAD) and the Petroleum Technology Development Fund (PTDF), Nigeria for funding this research work. Also, the Deutsche Forschungsgemeinschaft (DFG, German Research Foundation) -491183248 and Open Access Publishing Fund of the University of Bayreuth for funding this publication.

Data availability

Data will be made available on request.

References

[1] Zhang J, Zhang H-H, He Y-L, Tao W-Q. A comprehensive review on advances and applications of industrial heat pumps based on the practices in China. Appl Energy 2016;178:800–25.

[2] Farjana SH, Huda N, Mahmud MP, Saidur R. Solar process heat in industrial systems – a global review. Renew Sustain Energy Rev 2018;82:2270–86.

[3] H. AIT LAHOUSSINE OUALI, S. TOUILI, A. ALAMI MERROUNI, I. MOUKHTAR, Artificial neural Network-Based LCOH estimation for concentrated solar power plants for industrial process heating applications, Applied Thermal Engineering 236 (2024) 121810.

[4] Fan Y, Zhao X, Li J, Li G, Myers S, Cheng Y, et al. Economic and environmental analysis of a novel rural house heating and cooling system using a solar-assisted vapour injection heat pump. Appl Energy 2020;275:115323.

[5] Wang Z. Heat pumps with district heating for the UK's domestic heating: individual versus district level. Energy Procedia 2018;149:354–62.

[6] Arpagaus C, Bless F, Uhlmann M, Schiffmann J, Bertsch SS. High temperature heat pumps: Market overview, state of the art, research status, refrigerants, and application potentials. Energy 2018;152:985–1010.

[7] Hu B, Liu H, Jiang J, Zhang Z, Li H, Wang RZ. Ten megawatt scale vapor compression heat pump for low temperature waste heat recovery: Onsite application research. Energy 2022;238:121699.

[8] Wu X, Xing Z, He Z, Wang X, Chen W. Performance evaluation of a capacity-regulated high temperature heat pump for waste heat recovery in dyeing industry. Appl Therm Eng 2016;93:1193–201.

[9] Zhao Z, Gao S, Tian Y, Zhang H. Study on performance of high temperature heat pump system integrated with flash tank for waste heat recovery employed in steam production. Int J Energy Res 2021;45:20318–30.

[10] Pavlas M, Stehlík P, Oral J, Klemeš J, Kim J-K, Firth B. Heat integrated heat pumping for biomass gasification processing. Appl Therm Eng 2010;30:30–5.

[11] Jiang J, Hu B, Wang RZ, Deng N, Cao F, Wang C-C. A review and perspective on industry high-temperature heat pumps. Renew Sustain Energy Rev 2022;161:112106.

[12] Ganesan P, Eikevik TM. New zeotropic CO2-based refrigerant mixtures for cascade high-temperature heat pump to reach heat sink temperature up to 180 °C. Energy Convers Manage: X 2023;20:100407.

[13] Ma X, Du Y, Lei B, Wu Y. Energy, exergy, economic, and environmental analysis of a high-temperature heat pump steam system. Int J Refrig 2024.

[14] Zühlsdorf B, Bühler F, Bantle M, Elmegaard B. Analysis of technologies and potentials for heat pump-based process heat supply above 150 °C. Energy Convers Manage: X 2019;2:100011.

[15] Longo GA, Mancin S, Righetti G, Zilio C, Steven Brown J. Assessment of the low-GWP refrigerants R600a, R1234ze(Z) and R1233zd(E) for heat pump and organic Rankine cycle applications. Appl Therm Eng 2020;167:114804.

[16] Li S, Lu J, Yang H, Huang Z. Performance assessment and working fluid selection for heat recovery ejector heat pump system in cold climatic conditions. Int J Refrig 2024;158:313–28.

[17] Obika E, Heberle F, Brüggemann D. Thermodynamic analysis of novel mixtures including siloxanes and cyclic hydrocarbons for high-temperature heat pumps. Energy 2024;294:130858.

[18] Di Wu, B. Hu, R.Z. Wang, H. Fan, R. Wang, The performance comparison of high temperature heat pump among R718 and other refrigerants, Renewable Energy 154 (2020) 715–722.

[19] Kosmadakis G, Arpagaus C, Neofytou P, Bertsch S. Techno-economic analysis of high-temperature heat pumps with low-global warming potential refrigerants for upgrading waste heat up to 150 °C. Energ Conver Manage 2020;226:113488.

[20] Andersen MP, Zühlsdorf B, Markussen WB, Jensen JK, Elmegaard B. Selection of working fluids and heat pump cycles at high temperatures: Creating a concise technology portfolio. Appl Energy 2024;376:124312.

[21] Yan H, Hu B, Wang R. Air-source heat pump heating based water vapor compression for localized steam sterilization applications during the COVID-19 pandemic. Renew Sustain Energy Rev 2021;145:111026.

[22] Di Wu, Jiang J, Hu B, Wang RZ. Experimental investigation on the performance of a very high temperature heat pump with water refrigerant. Energy 2020;190:116427.

[23] Wang J, Belusko M, Evans M, Liu M, Zhao C, Bruno F. A comprehensive review and analysis on CO2 heat pump water heaters. Energy Convers Manage: X 2022;15:100277.

[24] Cui P, Yu M, Liu Z, Zhu Z, Yang S. Energy, exergy, and economic (3E) analyses and multi-objective optimization of a cascade absorption refrigeration system for low-grade waste heat recovery. Energ Conver Manage 2019;184:249–61.

[25] Jeßberger J, Arpagaus C, Heberle F, Brendel L, Bertsch S, Brüggemann D. Experimental investigations of upscaling effects of high-temperature heat pumps with R1233zd(E). Int J Refrig 2024;164:243–56.

[26] Spale J, Hoess AJ, Bell IH, Ziviani D. Exploratory Study on Low-GWP Working Fluid Mixtures for Industrial High Temperature Heat Pump with 200 °C Supply Temperature. Energy 2024;132677.

[27] Vannoni A, Sorce A, Traverso A, Fausto Massardo A. Techno-economic optimization of high-temperature heat pumps for waste heat recovery. Energ Conver Manage 2023;290:117194.

[28] Vieren E, Demeester T, Beyne W, Pihl Andersen M, Elmegaard B, Arteconi A, et al. Selection of pure and binary working fluids for high-temperature heat pumps: a financial approach. Appl Therm Eng 2024;252:123615.

[29] Hosseinnia SM, Poncet S, Nesreddine H, Monney D. Technical-economic-environmental analysis of high temperature cascade heat pump with R718 (high stage) and six different low global warming potential refrigerants (low stage). Energ Conver Manage 2023;292:117356.

[30] Fierro JJ, Hernández-Gómez C, Marenco-Porto CA, Nieto-Londoño C, Escudero-Atehortua A, Giraldo M, et al. Exergo-economic comparison of waste heat recovery cycles for a cement industry case study. Energy Convers Manage: X 2022;13:100180.

[31] Klamrassamee T, Kittijungjit T, Sukjai Y, Laoonual Y. Thermodynamic, economic, and carbon emission evaluation of various Organic Rankine cycle configurations for maximizing waste heat recovery potential. Energy Convers Manage: X 2025;26:100943.

[32] Abbas WKA, Vrabec J. Cascaded dual-loop organic Rankine cycle with alkanes and low global warming potential refrigerants as working fluids. Energ Conver Manage 2021;249:114843.

[33] Doninelli M, Di Marcoberardino G, Alessandri I, Invernizzi CM, Iora P. Fluorobenzene as new working fluid for high-temperature heat pumps and organic Rankine cycles: Energy analysis and thermal stability test. Energ Conver Manage 2024;321:119023.

[34] Wei F, Wang B, Cheng Z, Cui M. Experimental research on vapor-injected water source heat pump using R1234ze(E). Appl Therm Eng 2023;229:120595.

[35] Wei Y, Liu S, Yu J. A study on performance characteristics of vapor injection heat pump cycle with indirect heat recovery. Therm Sci Eng Prog 2022;34:101437.

[36] Bergamini R, Jensen JK, Elmegaard B. Thermodynamic competitiveness of high temperature vapor compression heat pumps for boiler substitution. Energy 2019;182:110–21.

[37] Navarro-Esbrí J, Mota-Babiloni A. Experimental analysis of a high temperature heat pump prototype with low global warming potential refrigerant R-1336mzz(Z) for heating production above 155 °C. International Journal of Thermofluids 2023;17:100304.

[38] Ma D, Sun Y, Ma S, Li G, Zhou Z, Ma H. Study on the working medium of high temperature heat pump suitable for industrial waste heat recovery. Appl Therm Eng 2024;236:121642.

[39] Ommen T, Jensen JK, Markussen WB, Reinholdt L, Elmegaard B. Technical and economic working domains of industrial heat pumps: Part 1 – Single stage vapour compression heat pumps. Int J Refrig 2015;55:168–82.

[40] Suong CO, Asanakham A. Evaluation of a single stage heat pump performance by figure of merit [FOM]. Energy Rep 2020;6:2735–42.

[41] Vieren E, Demeester T, Beyne W, Arteconi A, de Paepe M, Lecompte S. The thermodynamic potential of high-temperature transcritical heat pump cycles for industrial processes with large temperature glides. Appl Therm Eng 2023;234:121197.

[42] Mateu-Royo C, Navarro-Esbrí J, Mota-Babiloni A, Molés F, Amat-Albuixech M. Experimental exergy and energy analysis of a novel high-temperature heat pump with scroll compressor for waste heat recovery. Appl Energy 2019;253:113504.

[43] Lu Z, Gong Y, Yao Y, Luo C, Ma W. Development of a high temperature heat pump system for steam generation using medium-low temperature geothermal water. Energy Procedia 2019;158:6046–54.

[44] Di Wu, Jiang J, Hu B, Wang RZ, Sun Y. Experimental investigation and industrial application of a cascade air-source high temperature heat pump. Renew Energy 2024;232:121094.

[45] Querol E, Gonzalez-Regueral B, Ramos A, Perez-Benedito JL. Novel application for exergy and thermoeconomic analysis of processes simulated with Aspen Plus®. Energy 2011;36:964–74.

[46] Haydary J. Chemical process design and simulation: Aspen Plus and Aspen HYSYS applications, John Wiley & Sons. Hoboken, NJ: Inc; American Institute of Chemical Engineers; 2019.

[47] Jodeiri AM, Goldsworthy MJ, Buffa S, Cozzini M. Role of sustainable heat sources in transition towards fourth generation district heating – a review. Renew Sustain Energy Rev 2022;158:112156.

[48] Bamigbetan O, Eikevik TM, Nekså P, Bantle M, Schlemminger C. The development of a hydrocarbon high temperature heat pump for waste heat recovery. Energy 2019;173:1141–53.

[49] Loni R, Najafi G, Bellos E, Rajaee F, Said Z, Mazlan M. A review of industrial waste heat recovery system for power generation with Organic Rankine Cycle: recent challenges and future outlook. J Clean Prod 2021;287:125070.

[50] Kosmadakis G. Estimating the potential of industrial (high-temperature) heat pumps for exploiting waste heat in EU industries. Appl Therm Eng 2019;156:287–98.

[51] Marina A, Spoelstra S, Zondag HA, Wemmers AK. An estimation of the European industrial heat pump market potential. Renew Sustain Energy Rev 2021;139:110545.

[52] Papapetrou M, Kosmadakis G, Cipollina A, La Commare U, Micale G. Industrial waste heat: Estimation of the technically available resource in the EU per industrial sector, temperature level and country. Appl Therm Eng 2018;138:207–16.

[53] Höges C, Klingebiel J, Venzik V, Brach J, Roy P, Neumann K, et al. Low-GWP refrigerants in heat pumps: an experimental investigation of the influence of an internal heat exchanger. Energy Convers Manage: X 2024;24:100704.

[54] David LM, Barth M, Höglund-Isaksson L, Purohit P, Velders GJM, Glaser S, et al. Trifluoroacetic acid deposition from emissions of HFO-1234yf in India, China, and the Middle East. Atmos Chem Phys 2021;21:14833–49.

[55] Ma X, Du Y, Zhao T, Zhu T, Lei B, Wu Y. A comprehensive review of compression high-temperature heat pump steam system: Status and trend. Int J Refrig 2024;164:218–42.

[56] C. Arpagaus, S. Bertsch, Ntb Buchs, Experimental results of HFO/HCFO refrigerants in a laboratory scale HTHP with up to 150 °C supply temperature (2019).

[57] Khan M, Wen J, Shakoori MA, Liu Y. Condensation and thermophysical properties of R1336mzz(Z) through molecular dynamics simulations. Int J Refrig 2023;146:290–9.
[58] Huber ML, Lemmon EW, Bell IH, McLinden MO. The NIST REFPROP Database for Highly Accurate Properties of Industrially Important Fluids. Ind Eng Chem Res 2022;61:15449–72.
[59] Lemmon EW, Bell IH, Huber ML, McLinden MO. NIST Standard Reference Database: Reference Fluid Thermodynamic and Transport Properties-REFPROP, Version 10. National Institute of Standards and Technology: Standard Reference Data Program, Gaithersburg; 2018. p. 2018.
[60] ONU Environnement (ex-PNUE), Montreal Protocol on substances that deplete the ozone layer. 2022 Report of the Refrigeration, Air Conditioning and Heat Pumps Technical Options Committee (RTOC). 2022 Assessment, UNEP (United Nations Environment Programme), 2023.
[61] EPA, Transitioning to low-GWP alternatives in transport refrigeration, 2011, https://www.epa.gov/sites/default/files/2015-07/documents/transitioning_to_low-gwp_alternatives_in_transport_refrigeration.pdf.
[62] Zhai H, Shi L, An Q. Influence of working fluid properties on system performance and screen evaluation indicators for geothermal ORC (organic Rankine cycle) system. Energy 2014;74:2–11.
[63] ASHRAE Special Publications, ANSI/ASHRAE Addendum f to ANSI/ASHRAE Standard 34-2019.
[64] Astolfi M. Techno-economic Optimization of Low Temperature CSP Systems based on ORC with Screw Expanders. Energy Procedia 2015;69:1100–12.
[65] Fu L, Ding G, Su Z, Zhao G. Steady-state simulation of screw liquid chillers. Appl Therm Eng 2002;22:1731–48.
[66] Bamigbetan O, Eikevik TM, Nekså P, Bantle M, Schlemminger C. Theoretical analysis of suitable fluids for high temperature heat pumps up to 125 °C heat delivery. Int J Refrig 2018;92:185–95.
[67] Shah MM. An improved and Extended General Correlation for Heat transfer during Condensation in Plain Tubes. HVAC&R Research 2009;15:889–913.
[68] Petukhov BS. Heat transfer and Friction in Turbulent Pipe Flow with Variable Physical Properties. Elsevier 1970;6:503–64.
[69] Kern P. heat transfer. New York: McGraw-Hill; 1950.
[70] Gungor KE, Winterton R. A general correlation for flow boiling in tubes and annuli. Int J Heat Mass Transf 1986;29:351–8.
[71] Peters MS, Timmerhaus KD, West RE. Plant Design and Economics for Chemical Engineers. McGraw-Hill Education; 2003.
[72] Kapale UC, Chand S. Modeling for shell-side pressure drop for liquid flow in shell-and-tube heat exchanger. Int J Heat Mass Transf 2006;49:601–10.
[73] Andreasen JG, Baldasso E, Kærn MR, Weith T, Heberle F, Brüggemann D, et al. Techno-economic feasibility analysis of zeotropic mixtures and pure fluids for organic Rankine cycle systems. Appl Therm Eng 2021;192:116791.
[74] Farshi LG, Khalili S. Thermoeconomic analysis of a new ejector boosted hybrid heat pump (EBHP) and comparison with three conventional types of heat pumps. Energy 2019;170:619–35.
[75] Dixit M, Arora A, Kaushik SC. Thermodynamic and thermoeconomic analyses of two stage hybrid absorption compression refrigeration system. Appl Therm Eng 2017;113:120–31.
[76] Garousi Farshi L, Mahmoudi S, Rosen MA, Yari M, Amidpour M. Exergoeconomic analysis of double effect absorption refrigeration systems. Energ Conver Manage 2013;65:13–25.
[77] Mehr AS, Zare V, Mahmoudi S. Standard GAX versus hybrid GAX absorption refrigeration cycle: from the view point of thermoeconomics. Energ Conver Manage 2013;76:68–82.
[78] Jensen JK, Ommen T, Markussen WB, Reinholdt L, Elmegaard B. Technical and economic working domains of industrial heat pumps: Part 2 – Ammonia-water hybrid absorption-compression heat pumps. Int J Refrig 2015;55:183–200.
[79] Aminyavari M, Najafi B, Shirazi A, Rinaldi F. Exergetic, economic and environmental (3E) analyses, and multi-objective optimization of a CO2/NH3 cascade refrigeration system. Appl Therm Eng 2014;65:42–50.
[80] Robin S. Chemical process design and integration. John Wiley & Sons Ltd; 2005.
[81] Papapetrou M, Kosmadakis G, Giacalone F, Ortega-Delgado B, Cipollina A, Tamburini A, et al. Evaluation of the Economic and Environmental Performance of Low-Temperature Heat to Power Conversion using a reverse Electrodialysis – Multi-effect Distillation System. Energies 2019;12:3206.
[82] Statistisches Bundesamt, Daten zur Energiepreisentwicklung DESTATIS, 2023, https://www.destatis.de/DE/Themen/Wirtschaft/Preise/Publikationen/Energiepreise/energiepreisentwicklung-pdf-5619001.html, accessed 18 March 2024.
[83] Zhang Y, Zhang Y, Yu X, Guo J, Deng N, Dong S, et al. Analysis of a high temperature heat pump using BY-5 as refrigerant. Appl Therm Eng 2017;127:1461–8.
[84] o. bamigbetan, T.M. Eikevik, P. Nekså, M. Bantle, Review of vapour compression heat pumps for high temperature heating using natural working fluids, International Journal of Refrigeration 80 (2017) 197–211.
[85] o. bamigbetan, T.M. Eikevik, P. Nekså, M. Bantle, C. Schlemminger, Experimental investigation of a prototype R-600 compressor for high temperature heat pump, Energy 169 (2019) 730–738.
[86] Frate GF, Ferrari L, Desideri U. Analysis of suitability ranges of high temperature heat pump working fluids. Appl Therm Eng 2019;150:628–40.
[87] Fernández-Moreno A, Mota-Babiloni A, Giménez-Prades P, Navarro-Esbrí J. Optimal refrigerant mixture in single-stage high-temperature heat pumps based on a multiparameter evaluation. Sustainable Energy Technol Assess 2022;52:101989.
[88] White JA, Velasco S. Characterizing wet and dry fluids in temperature-entropy diagrams. Energy 2018;154:269–76.
[89] Zhang X, Li Y, Zhang Y, Zhang C. A method used to comprehensively evaluate dry and isentropic organic working fluids based on temperature-entropy (T-s) diagram. Energy 2023;263:125855.
[90] Heberle F, Brüggemann D. Thermo-Economic Analysis of Zeotropic Mixtures and Pure Working Fluids in Organic Rankine Cycles for Waste Heat Recovery. Energies 2016;9:226.
[91] Gilbert T, Menon AK, Dames C, Prasher R. Heat source and application-dependent levelized cost of decarbonized heat. Joule 2023;7:128–49.
[92] Vieren E, Demeester T, Beyne W, Magni C, Abedini H, Arpagaus C, et al. The potential of Vapor Compression Heat Pumps Supplying Process Heat between 100 and 200 °C in the Chemical Industry. Energies 2023;16:6473.
[93] Menin L, Borelli G, Prada A, Pernigotto G, Gasparella A, Baratieri M. Decarbonization of space heating in the Italian Alpine context: Thermo-economic assessment of the levelized energy cost of heating under alternative renewable scenarios. Energy Convers Manage: X 2025;25:100886.